IEEE Access
Multidisciplinary : Rapid Review : Open Access Journal

Received 7 November 2024, accepted 30 November 2024, date of publication 5 December 2024, date of current version 6 January 2025.

Digital Object Identifier 10.1109/ACCESS.2024.3512201

RESEARCH ARTICLE

A Highly Compact Split Ring Resonator-Based Rectangular Dielectric Resonator Antenna With Multiband Characterization

SHAHID KHAN[1], OWAIS KHAN[2], KIRAN RAHEEL[3], SYED AHSON ALI SHAH[4], (Member, IEEE), BILAL TARIQ MALIK[1], SALAHUDDIN KHAN[5], NEELAM GOHAR[6], AND SLAWOMIR KOZIEL[1,7], (Fellow, IEEE)

[1]Faculty of Electronics, Telecommunications and Informatics, Gdánsk University of Technology, 80-233 Gdánsk, Poland
[2]Department of Electrical and Computer Engineering, COMSATS University Islamabad, Abbottabad Campus, Abbottabad 22060, Pakistan
[3]Department of Electrical Engineering, CECOS University of IT and Emerging Sciences, Peshawar 25000, Pakistan
[4]Graduate School of Energy Convergence, Gwangju Institute of Science and Technology, Gwangju 61005, South Korea
[5]College of Engineering, King Saud University, Riyadh 11421, Saudi Arabia
[6]Department of Computer Science, Shaheed Benazir Bhutto Women University, Peshawar 25000, Pakistan
[7]Engineering Optimization and Modeling Center, Reykjavik University, 101 Reykjavik, Iceland

Corresponding authors: Shahid Khan (shahid.khan@pg.edu.pl) and Slawomir Koziel (koziel@ru.is)

This work is partially supported by the National Science Centre of Poland Grant 2020/37/B/ST7/01448, by the Nobelium Joining Gdansk Tech Research Community DEC-17/2021/IDUB/I.1 and by the Icelandic Research Fund Grant 2410297. The authors sincerely appreciate funding from Researchers Supporting Project number (RSP2025R58), King Saud University, Riyadh, Saudi Arabia.

ABSTRACT This work encompasses a novel highly compact Split Ring Resonator (SRR) based quad-band Dielectric Resonator Antenna (DRA) for 4G and 5G applications. The proposed antenna comprises of an extended rectangular feedline and a rectangular DR in combination with two SRRs. The DRA uses the extended rectangular microstrip feedline for providing better impedance matching and enhanced performance. Remarkably, the introduction of SRRs on either side of the feedline enables the DRA to resonate at four distinct frequency bands, i.e., 1.62 GHz, 3.03 GHz and 4.7 GHz and 6.56 GHz respectively. The two lower operating bands with narrow band response are due to SRRs while two upper bands with wide band characteristics are due to rectangular DR. The simulated performance of the rectangular DRA is validated through measurements, performed on a fabricated prototype. At the corresponding resonance frequencies, the suggested design exhibits −10 dB impedance bandwidths of 9.2%, 5%, 8.3%, and 5.6%. With a notable peak gain of 2.3 dBi and an efficiency of 93%, the suggested design has excellent radiation pattern stability. To the best of authors knowledge, this is the first design where SRRs are incorporated with rectangular DR to achieve multiband operations. The simulated and measured findings show a strong agreement, highlighting the SRR-based DRA appropriateness for multiband wireless applications (such as satellite television, radio astronomy, Bluetooth, WiFi, and 6G), while demonstrating its significant contribution to the field.

INDEX TERMS SRR, DRA, multiband, 4G, 5G, bluetooth and Wi-Fi.

I. INTRODUCTION

Due to the recent major advancements in wireless communication technologies, multifunctional antennas are widely used in a variety of wireless gadgets. To facilitate common users, a variety of wireless communication standards with different working frequency bands are in use. These include wireless local area networks (WLAN), third generation (3G) and fourth generation (4G) mobile communication networks, long-term evolution (LTE), and worldwide interoperability for microwave access (WiMAX). In addition, the fifth-generation (5G) communication systems, already in use

The associate editor coordinating the review of this manuscript and approving it for publication was Ali Karami Horestani.

© 2024 The Authors. This work is licensed under a Creative Commons Attribution 4.0 License.
For more information, see https://creativecommons.org/licenses/by/4.0/

in many countries provide exceptional advantages, such as higher data rate, lower latency, wider bandwidth, high gain and low energy consumption. Therefore, antennas with multiband characteristics are highly preferred for next generation communication systems [1].

Numerous methods have been put forth in the literature, which enable single element DRAs with multiband characteristics. A straightforward and efficient method of achieving multiband functioning is to stack numerous DRs with varying permittivity [2]. Varying size and permittivity of each DR, provides independent control over the resonant frequencies of each band. Additional resonant frequencies are also produced by adding metallic strips or slots to the DRA [2]. Coupling with the DR, the parasitic elements produce new resonant modes generating multiband responses. In case of narrow bandwidth, aperture-coupled feeding can be opted to enhance the bandwidth while reducing spurious radiation of DRAs [1]. Several resonant frequencies are obtained by carefully planning the aperture's size and shape. The high radiation efficiency, low dielectric losses, tunable bandwidth, small size, and variety of feeding techniques have garnered more attention towards dielectric resonator antennas (DRAs) [3]. In order to produce multiband characteristics, various DRAs with various frameworks and feeding methods have recently been proposed. These methods include the use of parasitic elements with a resonating structure [4], multimode excitation techniques (which allow the generation of fundamental and higher order modes at various required bandwidths) [5], [6], [7], [8], and hybrid DRAs, which combine DRs with patch or monopole antennas [9], [10], [11], [12].

The hybrid DRA technique is one of the widely used methods for generating multiband responses. For multiband applications, a hybrid Z-shaped cylindrical DRA has been suggested in [9]. Additionally, a multiband DRA fed by a slot with a Minkowski fractal structure has been suggested in [11]. Due to low radiation and dispersion losses, choosing a coplanar waveguide (CPW) feeding network is also an excellent way to get wide and multiband responses [13], [14], [15]. DRAs with a variety of shapes, such as cylindrical [4], [5], [12] and rectangular [15], [16], [17], have previously been reported for wide and multiband applications.

In [18], a mountable multiband dielectric resonator is investigated for wireless communication. The $50 \times 50 \times 1.6$ mm^3 sized design contains resonant frequencies with ranges 5.04–6.13 GHz, 6.87–7.97 GHz, and 8.58–9.63 GHz. The suggested design features an extremely large DR geometry, along with a complicated structure. Additionally, a rectangular shaped hybrid DRA with $60 \times 60 \times 1.6$ mm^3 volume for multiband operations has been proposed in [19]. The stated design has a rectangular DR. Due to enormous DR size and extremely low radiation efficiency, the recommended antenna design is not helpful for real-time applications. A frequency reconfigurable dielectric resonator antenna for multiband operation is examined in [20]. The reported design has a geometry of 47×50 mm^2, resonating at 2.06 GHz and 5.51 GHz with a return loss of −30 dB and −15 dB, respectively. The proposed design offers only two operating bands with a very complex geometry. Various DRA designs with modified structures including multiple DRAs [8], [9] with wideband response, C-shaped DRAs [13], [23], and fractal DRAs [7], [21], [22] are also reported in the literature. However, this choice may increase the production and cost of DRAs. On the other hand, RDRA providing an ease in fabrication and two degrees of freedom is a viable solution. The majority of DRAs that have been published are either large or lack multiband coverage. This reduces their significance for many wireless applications. Therefore, simple, small, high performance multiband DRAs need to be investigated for advanced communication systems.

Numerous techniques for improving the performance and working of multiband antennas have been investigated. Amongst them, one is Defected Ground Structure (DGS) [24]. In this technique, different shaped slots are created in the ground plane to enhance bandwidth and gain. These slots are rectangular, square or L shaped as described in [25], [26], and [27]. Each slot is having different length, which alternates the current flow, corresponding to different operating frequency. Shape and orientation of the slots also plays pivotal role in determining the operating frequency and performance of an antenna. Along DGS, complementary split ring resonators (CSSRs) and split ring resonators (SRRs) have been widely explored for achieving high gain and multiband operations. In [28], a hemispherical shaped DRA, based on metamaterial is employed to increase the gain. The design resonates at 3.6 GHz with $60 \times 60 \times 1.6$ mm^3 overall size. Gain augmentation is achieved by incorporating an array of 5×5 unit cells with the DR. The design has augmented the gain but no increment in number of operating bands is witnessed. In [29] a hexagon shaped SRR metamaterial is employed for reducing mutual coupling in MIMO antenna system. The 40×40 mm^2 geometry of the suggested design has an enhanced isolation of −30 dB. The proposed architecture achieves a single operating band at 5.2 GHz. The work in [30] reports a circular dielectric resonator antenna fed by microstrip line. The design is $40 \times 40 \times 1.6$ mm^3 in size and has a central frequency at 5.2 GHz. Gain is increased by using an EBG surface of 75×75 mm^2 below the antenna element. The proposed antenna system with metamaterial has a single band with complex architecture.

It is significant to know that in the absence of additional technique, alone RDRA arrangement cannot provide miniaturization and multiband operations. Despite significant progress in multiband antennas, limitations remain across designing the miniaturized RDRA for multiband wireless applications. Notably, achieving sufficient miniaturization and multiple operating bands while keeping the gain acceptable for wireless applications proves challenging. This tradeoff between miniaturization, multiband performance, and design simplicity restricts the widespread adoption of

MOST WIEDZY Downloaded from mostwiedzy.pl

RDRA in wireless technology. The novelty of our design lies in intelligently using the SRRs in combination with RDR to create a less complex structure with the provision of multiband operation and highly compact size. The design is highly miniaturized as compared to other published multiband antennas. From a performance perspective, our design has four resonance frequencies, high gain, minimum group delay and stable link budget analysis. These features and multiband characteristics make the design novel and useful for the desired wireless applications.

This paper proposes a comprehensive solution to address issues related to multiband operation, and acceptable performance within a compact-sized design. A single port miniaturized SRR based RDRA design having dimensions of 56 × 55 × 6.6 mm^3 is proposed for multiband wireless applications. To reduce the antenna size, the proposed RDRA utilizes the SRRs. On the other hand, DR cutting into different shapes commonly employed in the miniaturization of RDRA are avoided thereby making the design fabrication easy and low-cost. Furthermore, the suggested design uses coplanar waveguide (CPW) feedline, which makes all the component of the proposed design available on the same surface. The performance of the proposed antenna has been evaluated in terms of antenna parameters (S-parameters, radiation patterns, group delay, and link budget analysis). These parameters are found to be within the acceptable ranges. To the best of the authors' knowledge, the proposed design is the first compact SRR based RDRA design proposed for miniaturization and multiband applications. Compared to existing multiband antennas, the proposed design exhibits a significantly smaller footprint while maintaining acceptable performance.

From the literature it is evident that there is a lack of research on the use of SRRs in combination with dielectric resonator antennas for achieving multiband operations at sub 6 GHz band. Thus, the aim of our work is to combine SRR with RDR for achieving a low cost, compact, multiband RDRA. The following are the major contributions of the proposed work:

1. To the best of authors knowledge, SRRs have been used for the first time with RDR to generate multiband operations.
2. To the best of authors knowledge, this is the compact multiband DRA with four operating bands.
3. Detailed analysis of DR and SRR design is presented.
4. To the best of authors knowledge, for the first time link budget analysis is presented for multiband DRA.
5. A comparison of the simulated results from CST and equivalent circuit from ADS is presented.
6. A detailed comparison between recently published works and proposed design is detailed, confirming the novelty of the proposed design.

The remaining work is organized as follows: The design process of the proposed antenna is presented in Section II. Section III deals with the parametric analysis. Section IV evaluates the measurement and simulation outcomes. Section V analyzes the link budget, and Section VI concludes the work.

II. DESIGN AND METHODOLOGY

A. ANTENNA CONFIGURATION

Fig. 1 (a) and (b) shows the proposed antenna design top and split side views respectively. The suggested DRA is placed on an economical FR4 substrate that has a loss tangent of 0.025 and a dielectric constant of 4.3. The complete dimensions of the substrate are Ls × Ws × hs, where Ls, Ws, and hs stand for the substrate's length, width, and height, respectively. Rectangular DR, which is an important part of the proposed design is placed atop the extended feedline. DR is made of ceramic material with $\epsilon_r = 10$. The DR have dimensions of $L_d \times W_d \times H_d$ which are the length, width, and height of the DR respectively. The DR is excited by quarter wave transformer followed by an extended rectangular shaped feedline. For better impedance matching, the feedline with 2.9 mm width is optimized at 50Ω impedance. To excite the DR with multiband responses, the single feedline is symmetrically expanded below the DR. Moreover, the height of the DR is kept 5 mm, which portrays the proposed design compactness at lowest cut-off frequency. For the multiband operations, a pair of square loop shaped split ring resonators (L-SRRs) are introduced symmetrically along the feedline. The detailed dimensions of the proposed design are listed in Table 1.

B. DESIGN PROCEDURE

The proposed DRA is based on certain design equations, which are detailed in this section. The design equations are based on two important entities, the first one is DR and the second one is SRR. The first set of equations are incorporated to characterize the DR dimensions. The second set of equations are associated with the design of the split ring resonator.

1) DESIGN EQUATIONS FOR DIELECTRIC RESONATOR ANTENNA

The DRA design follows dielectric waveguide model (DWM) as both structures have many common features. As DRA has no separate theory, thus theoretical resonance frequency of a dielectric resonator antenna is calculated using DWM equations as follows [31], [32]:

$$k_x = \frac{\pi}{L_d} \tag{1}$$

$$k_y = \frac{\pi}{W_d} \tag{2}$$

$$k_z \, tan\left(\frac{k_x d}{2}\right) = \sqrt{(\epsilon_0 \epsilon_r - 1)\, k_0^2 - k_z^2} \tag{3}$$

$$k_x^2 + k_y^2 + k_z^2 = \epsilon_0 \epsilon_r k_0^2 \tag{4}$$

$$f_r = \frac{c}{2\pi\sqrt{\epsilon_0}\epsilon_r}\sqrt{k_x^2 + k_y^2 + k_z^2} \tag{5}$$

MOST WIEDZY Downloaded from mostwiedzy.pl

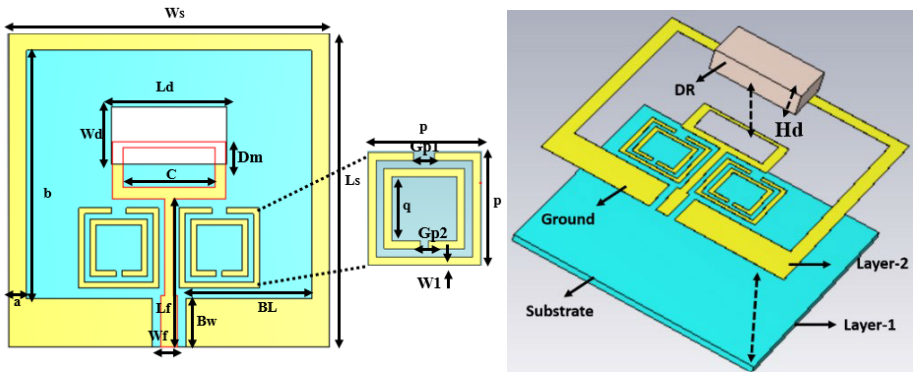

(a) (b)

FIGURE 1. Detailed structure of proposed antenna (a) Front view (b) Exploded view.

TABLE 1. Optimized dimensions of proposed design.

Parameter	Dimension (mm)	Parameter	Dimension (mm)	Parameter	Dimension (mm)
W_S	56	L_s	55	H_s	1.6
a	3	H_d	5	p	14
b	43.5	L_f	26	q	10
C	20	W_f	2.8	$Gp1$	2.6
L_d	20	BL	22.5	$Gp2$	1
W_d	10	Bw	8.5	$W1$	1

where c is the speed of light ; ϵ_r is the relative permittivity of the DRA and fr is the operating frequency. k_x, k_y, and k_z represent the wave numbers across L_d, W_d and H_d which are the length and width and height of the rectangular dielectric resonator antenna respectively. By using equation (5), the resonant frequency of rectangular DR is calculated and found to be 3.9 GHz. Depending on the type of feed line and hybrid nature of the DR, the initial resonance frequency may be shifted as compared to the calculated one.

2) DESIGN EQUATIONS FOR SPLIT RING RESONATOR

The structure and dimensions of the square split double ring resonator is shown in Fig. 1(b) and Table 1 respectively. It consists of two square rings with a gap between them. Here p and q denote the widths of the outer and inner sides of the square respectively. $W1$ denotes the width of the conductor. The dielectric width between the inner and the outer square is g = 1 mm while G_P1 and G_p2 denote the SRR split gaps.

Current flow originates from the ring's ability to conduct when a magnetic field is applied perpendicular to the ring plane. Mutual capacitances result from the dielectric gaps between the rings and the current passing through them, which allows the rings to function as an inductor. As a result, a parallel LC tank circuit will be an equivalent representation of the SRR [32].

We can calculate the resonant frequency as:

$$f_o = \frac{1}{2\pi\sqrt{LC}} \tag{6}$$

where C is the equivalent capacitance and L is the effective inductance due to both rings.

$$L = \frac{4.86\mu_0}{2}(p - W1 - g)\left[ln\left(\frac{0.98}{\rho}\right) + 1.84\rho\right] \tag{7}$$

where,

ρ is the filling factor of the inductance and is given by:

$$\rho = \frac{W1 + g}{p - W1 - g} \tag{8}$$

The effective capacitance is given by

$$C = \left(p - \frac{3}{2}(W1 + g)\, C_{pul}\right) \tag{9}$$

where,

MOST WIEDZY Downloaded from mostwiedzy.pl

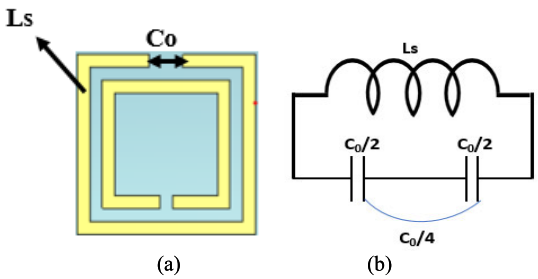

FIGURE 2. (a) Topology of square SRR (b) Equivalent circuit model.

C_{pul} is the per unit length capacitance between the rings which is given as:

$$C_{pul} = \varepsilon_0 \varepsilon_{eff} \frac{K\left(\sqrt{1-k^2}\right)}{K(k)} \tag{10}$$

where,

ε_{eff} is the effective dielectric constant which can be expressed as:

$$\varepsilon_{eff} = \frac{\varepsilon_r + 1}{2} \tag{11}$$

K(k) denotes the complete elliptical integral of the first kind with k expressed as:

$$k = \frac{g}{g + 2W1} \tag{12}$$

Using above expressions, the lumped model equivalent circuit of the SRR is designed which is shown in Fig. 2.

Due to the SRR's high electrical conductivity, induction is mitigated by the capacitance that exists across the rings. The SRR is a kind of metamaterial architectures that generates a negative permeability (-μ) upon exposure to an axial magnetic field, among the several forms of left-handed materials (LHM) [33].

3) DESIGN EVOLUTION

The detailed design process of the SRR-based DRA is demonstrated in Fig. 3. Four important steps are involved in completing the specified configuration, each of which adds to the desired antenna performance. Fig. 4 shows the simulated reflection coefficients for each step.

As shown in Fig. 3 (a), step 1 concentrates on the excitation of the rectangle DR with a simple microstrip feedline. As seen in Fig. 4, the DR resonates with the basic operating modes and has a single resonant frequency with comparatively high impedance matching at 2.1 GHz. To excite the DR symmetrically, the feedline is evenly divided and expanded below the DR in step 2. This step generates two wide bands. Step 3 includes adding an SSR on one side of the feedline, which introduces an extra band, enabling the design to resonate at three bands. To enhance the impedance matching and add an extra band, step 4 introduces another SRR on the right side of the feedline. As both SRRs are have similar structure and positioned symmetrically, thus addition of second SRR helps to add another band with enhanced impedance matching. At this stage, the DRA exhibits four operating bands. The lower bands with narrow band response are due to SRRs and higher bands with wideband responses are due to the hybrid DR. Interestingly the extended patch below the DR also acts as an independent resonant structure. Fig. 4(b), shows that without DR the patch accompanied by SRRs generate three operating bands while adding DR not only add another band but also improve the overall gain of the resonance frequencies as shown in Fig. 4(c).

4) EQUIVALENT CIRCUIT

The equivalent circuit determination for the proposed multi-band DRA is based on important parameters such as feeding mechanism, shape and substrate of DRA, and number of SRRs. The lumped circuit model is the alternative way to express the similar behavior of the DRA through an equivalent circuit consists of inductance (L), Capacitance (C) and Resistance (R). The equivalent circuit of DRA and SRR is presented as a parallel combination of RLC circuit elements as shown in Fig. 5. In case of multiband DRA, the equivalent circuit is based on multiple cascaded RLC circuits. SRRs are excited through mutual coupling and resonate independently. The transmission line inductance (L_0) and capacitance (C_0) at resonance frequency is calculated using equation 6, 13 and 14. The remaining lumped circuit elements are calculated using equations 15 and 16. The imaginary values helpful in determining the lumped elements calculation are imported from CST (Computer Simulation Technology). Once all these circuit elements are calculated, ADS (Advanced Design System) simulation tool is used to validate the S11 from CST. Fig. 3b shows that S11 from CST and ADS are in close agreement. The values calculated for the DRA and SRR circuit are as: Lo = 0.202 nH, Co = 0.13 pF, R1 = 42.14 Ω, L1 = 0.98 nH, C1 = 6.56 pF, R2 = 32.8 Ω, L2 = 1.631 nH, C2 = 4.126 pF, R3 = 33.22 Ω, L3 = 0.233 nH, C3 = 2.6 pF, R4 = 44.17 Ω, L4 = 0.61 nH, C4 = 2.71 pF, R5 = 62.33 Ω, L5 = 0.23 nH, C5 = 0.94413 pF.

The values of equivalent capacitance and inductances can be calculated using the following equations 13-22 [43].

$$L_0 = 100h\left(4\sqrt{\frac{W_f}{h}} - 4.21\right) \tag{13}$$

$$C_0 = W_f\left[(9.5\varepsilon_r + 1.25)\frac{W_f}{h} + 5.2\varepsilon_r + 7\right] \tag{14}$$

$$L = \frac{img\,(Z_{11})}{2\pi f} \tag{15}$$

$$C = \left[(2\pi f)^2 L\right]^{-1} \tag{16}$$

where Z_{11} is the port impedance for S_{11} and W_f is the width of feedline. Now this port impedance for a specific resonance frequency is detailed as:

First, convert the S11 into input impedance as:

$$Z_{in}, i = Z_0\frac{(1 + S_{11}, i)}{(1 - S_{11}, i)} \quad \text{where, i} = 1, 2, 3 \text{ and } 4 \tag{17}$$

MOST WIEDZY Downloaded from mostwiedzy.pl

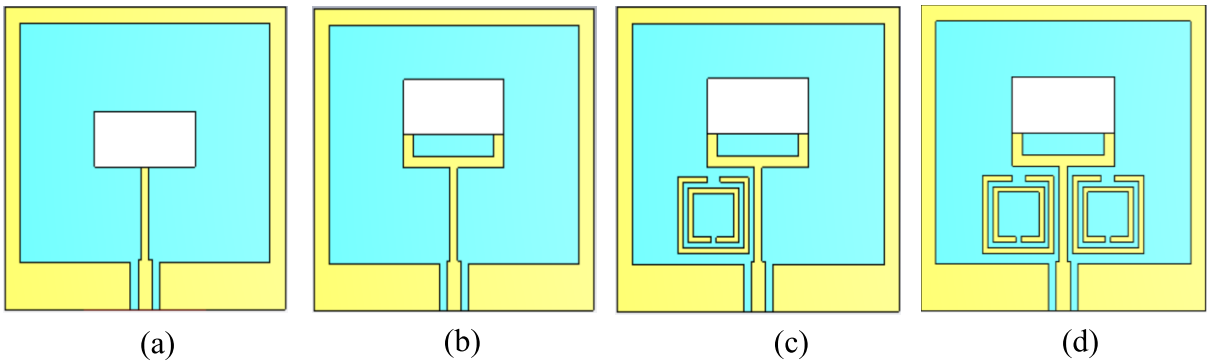

FIGURE 3. Design evolution steps.

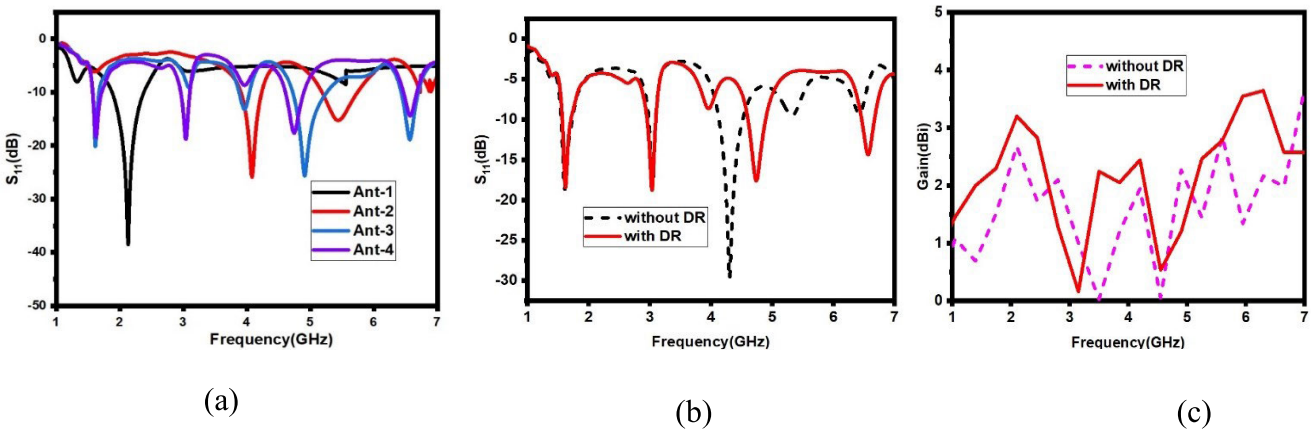

FIGURE 4. (a) Shows the proposed antenna results in each successive steps, (b) shows the S11 response without and with DR and (c) shows the gain of the proposed design without and with DR.

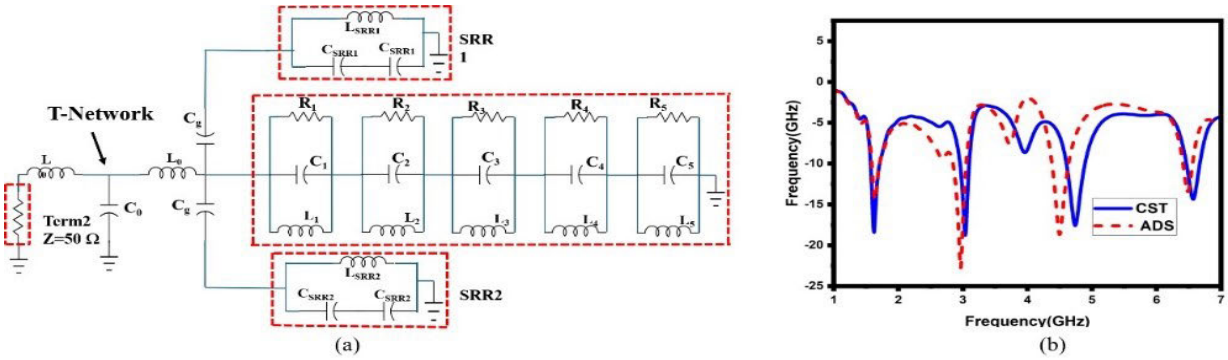

FIGURE 5. (a) Equivalent circuit (b) Simulated S11 results comparison of CST and ADS.

For ease in understanding, equation 17 has an alternative representation as:

$$Z_{in} = Z_0 \frac{[Z_L + jZ_0 tan(\beta l)]}{[Z_0 + jZ_L tan(\beta l)]} \tag{18}$$

where,

β is the propagation constant and l is the feedline length. In the next step we separate the input impedance into real and imaginary values as:

$$Z_{in}, i = R_{in}, i + jX_{in}, i \tag{19}$$

where R_{in}, i is the radiation resistance of the *ith* resonance frequency and jX_{in}, i is the reactance of the *ith* resonance frequency.

If the value of jX_{in}, i is positive, the reactance is inductive which can be calculated as:

$$X_{in,i} = \omega_i L_i \Rightarrow L_i = \frac{X_{in,i}}{\omega_i} \tag{20}$$

And in case jX_{in}, i is negative then the reactance is capacitive which can be calculated as:

$$X_{in,i} = -\frac{1}{\omega_i C_i} \Rightarrow C_i = -\frac{1}{\omega_i X_{in,i}} \tag{21}$$

MOST WIEDZY Downloaded from mostwiedzy.pl

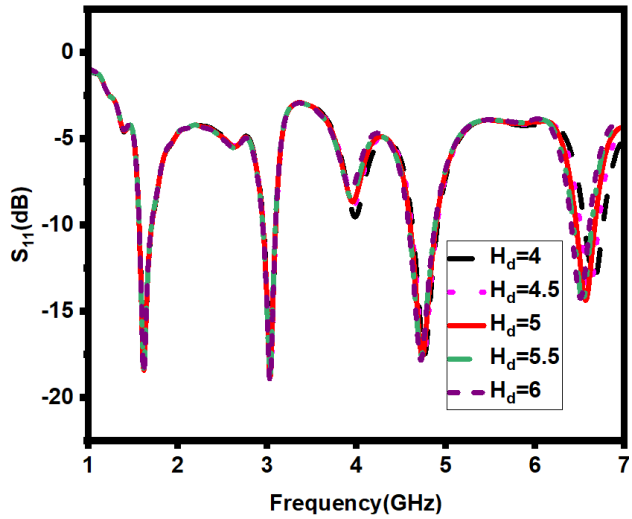

(a)

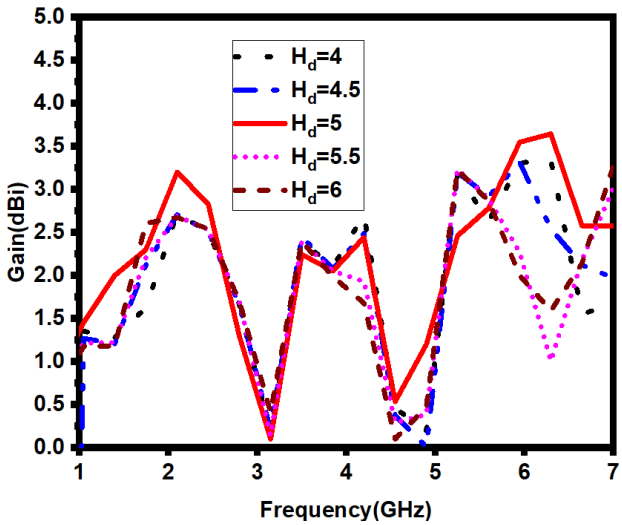

(b)

FIGURE 6. Proposed antenna results in each successive steps. (a) Reflection coefficient (b) Gain vs frequency.

and finally, resonance frequency for each branch can be calculated as:

$$f_i = \frac{1}{2\pi\sqrt{LiCi}} \tag{22}$$

For all four-resonance frequencies, the four parallel RLC circuits will then be cascaded to make the equivalent circuit. It is also important to note that SSRs are also equivalent to RLC circuits but have no physical connection with feedline thus they add their part through capacitive coupling which is shown in Fig. 5(a).

III. PARAMETRIC STUDY

A thorough parametric study is carried out to evaluate the influence of different critical parameters on the simulated outcomes of the suggested design. These parameters encompass DR height (H_d), length of the SRR (p), width of the SRR (W_1), vertical width of the ground plane (a) and the length of the feedline (L_f).

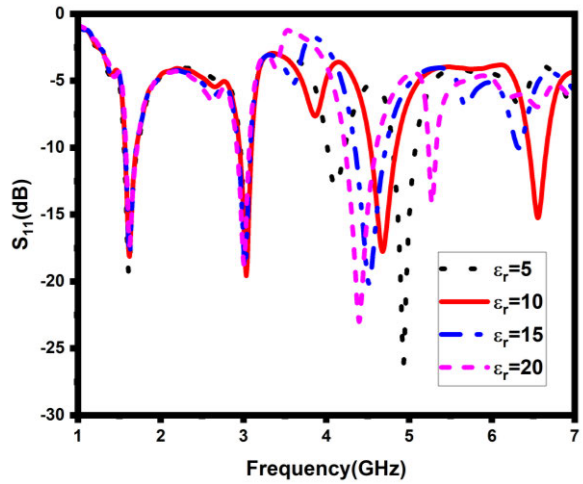

FIGURE 7. Impact of permittivity "ϵ_r" of the material.

A. EFFECT OF ANTENNA DESIGN PARAMETERS ON REFLECTION COEFFICIENT

The overall compactness of the design is mostly dependent on the height of the DR. The impact of varying DR height on the reflection coefficients is seen in Fig. 6 (a). The findings unequivocally show that a rise in the DR height causes the top operational band to migrate downward. This change is consistent with the DR's analytical formula, confirming its effect on the operational frequency range. Furthermore, the trend shown for the upper band supports the DRA's predicted behavior. This analysis also shows that higher band is highly controlled by the DR dimensions as compared to the other bands which are largely unaffected by varying the DR dimensions. For the suggested DRA, a height of 5 mm is determined to be the ideal value based on the |S11| response and the materials availability. This selection guarantees an appropriate harmony between the desired operating frequency range and compactness. Fig. 6(b) explains the impact of DR height on the gain of the proposed design. From the figure, it is clear that increasing the DR height increases the gain due to increase in effective area of the DR. The maximum gain is attained at the DR height of 5 mm. Any further increment in DR height results in a decrease of the proposed design gain.

Fig. 7 describes the impact of the material permittivity on reflection coefficients. It is evident that selecting the DR with relative permittivity 10 achieves more bands with better impedance matching. A right shift in frequencies is also noticed due to inverse relation of frequencies with the permittivity of the DR. Materials with high permittivity are more expensive, thus selecting DR with low permittivity helps to keep the design low cost.

Fig. 8(a) presents the influence of SRR outer loop area on the reflection coefficients while Fig. 8(b) represents the influence of SRR outer loop area on the gain of the design.

MOST WIEDZY Downloaded from mostwiedzy.pl

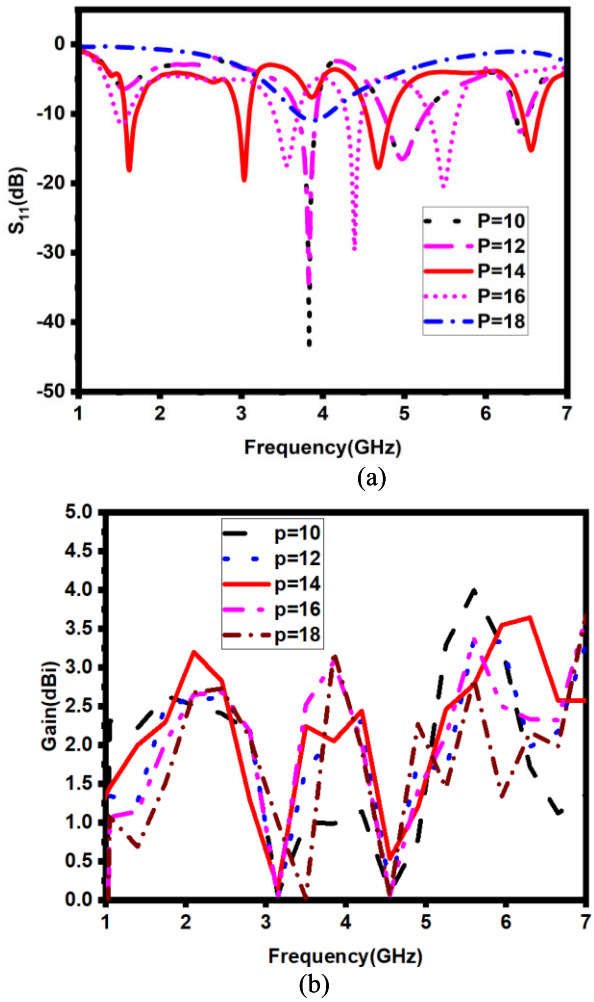

FIGURE 8. Impact of SRR outer loop area "p" on (a) reflection coefficient (b) on Gain of the proposed design.

The visualization makes it clear that changing the area has an impact on the operating bands as well as impedance matching. The DRA performs better when the SRR area is increased as it improves the impedance matching. The SRR with an area (p × p) of 14 mm^2 give the lager number of functioning bands with good impedance matching. Reduced impedance matching is the outcome of any further increase in the area of SRR. By ensuring an efficient link between the SRR and the DR, this ideal value promotes better performance. Furthermore, the effect of SRR area is also shown on the gain performance. From the Fig. 8(b), it is evident that with a compact SRR area, the design has a low gain performance on resonating frequencies. Gradually increasing SRR area until p is 14 mm, has improved the gain of the proposed design at resonance frequencies to 1.4 dBi, 1.8 dBi, 2 dBi and 2.1 dBi respectively. Any further increment in the area of SRR (p), reduce the design gain performance.

Fig. 9 also examines the impact of the ground plane vertical width, which causes the operational band to move towards lower frequencies. The surface current distribution during coupling influences the DRA's overall resonant behavior.

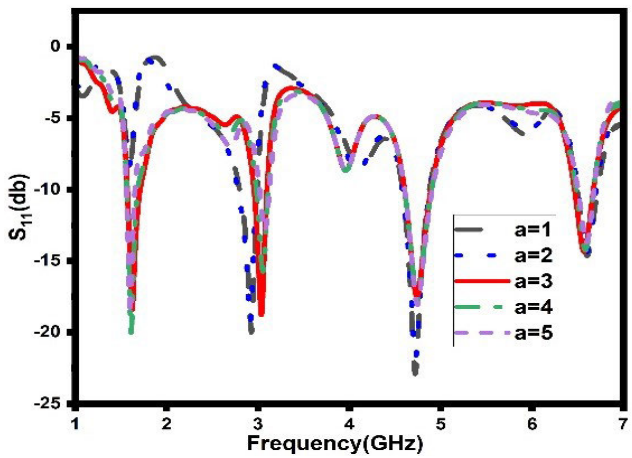

FIGURE 9. Impact of vertical width of ground plane "a" on reflection coefficient.

After taking into account the available space and the value of the reflection coefficients a width of 3 mm is chosen.

Similarly, Fig. 10(a) and (b) details the impact of the SRR loop width on the impedance matching and gain of the operating bands respectively. Fig. 10(a) shows that SRR width has a minor impact on impedance matching and any shift in the operating bands. Fig 10(b) explains the impact of SRR width on the gain of the design. It is shown that by gradually increasing the SRR loop width from 0.8 mm to 1 mm, enhances the gain at resonance frequencies. A maximum gain augmentation is noticed at 1 mm thickness of SRR patch. Fig. 11 shows the impact of changing feedline length on the reflection coefficients. Increasing the length of the feedline modifies the resonant behavior of the DRA. The design shows the larger number of operating bands with appropriate impedance matching at 26 mm feedline length. This ideal length achieves good impedance matching over the entire operating band and guarantees the intended multiband performance.

Fig. 12 shows the impact of changing DRA position over the extended rectangular feed line structure "D_m". It is seen from that, the bandwidth span increases slightly as we increase the value of this parameter.

IV. SIMULATED AND MEASURED RESULTS

This section details the suggested design final simulation and measurement data, offering a thorough assessment of its performance. Reflection coefficients, mutual impedances, gain and efficiency, current distribution, and radiation patterns throughout the operating bands are among the important evaluated variables.

A. EXPERIMENTAL SETUP

CST Microwaves Studio software is used to fully model, simulate, and assess the suggested SRRs based DRA design. Thus, performance of the antenna system may be accurately assisted using this electromagnetic modeling tool. Experimental measurements are carried out on the fabricated

MOST WIEDZY Downloaded from mostwiedzy.pl

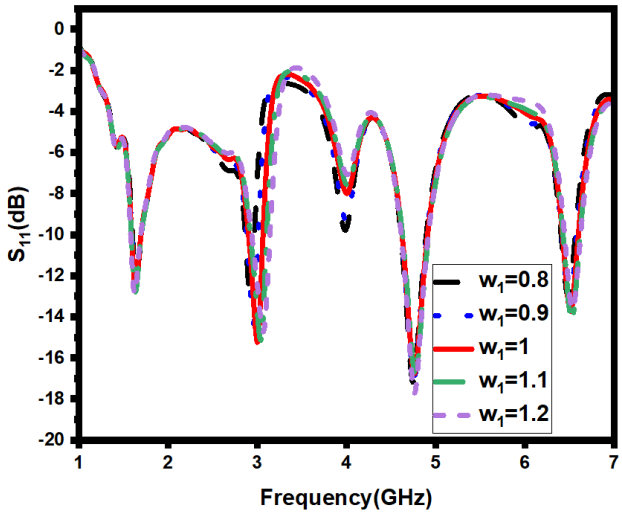

(a)

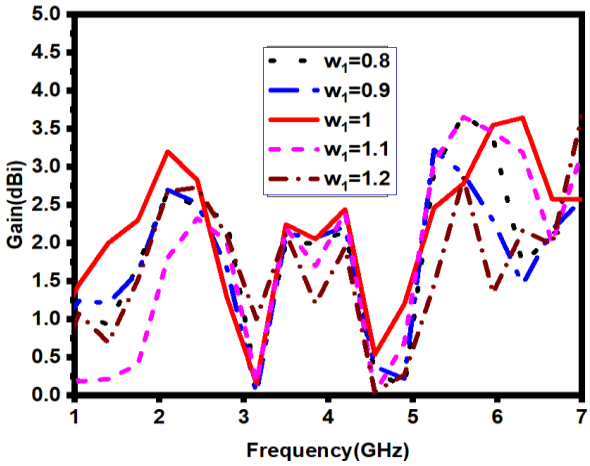

(b)

FIGURE 10. Impact of width of SRR loop "W_1" (a) on reflection coefficients, (b) on the gain of the proposed design.

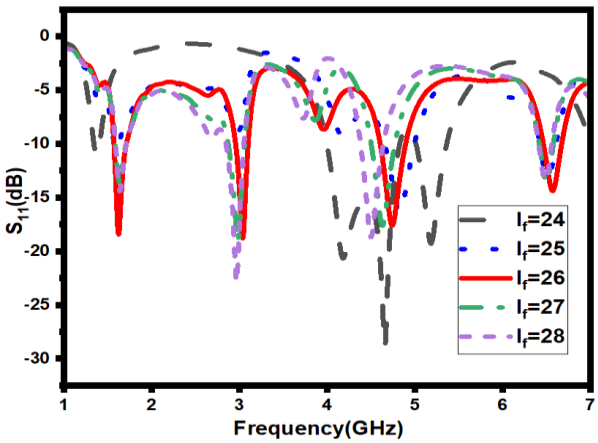

FIGURE 11. Impact of feedline length "L_f" on reflection coefficient.

prototype, which verifies the simulated results. For an accurate assessment of the antenna's performance, an anechoic chamber, an environment devoid of outside reflections and

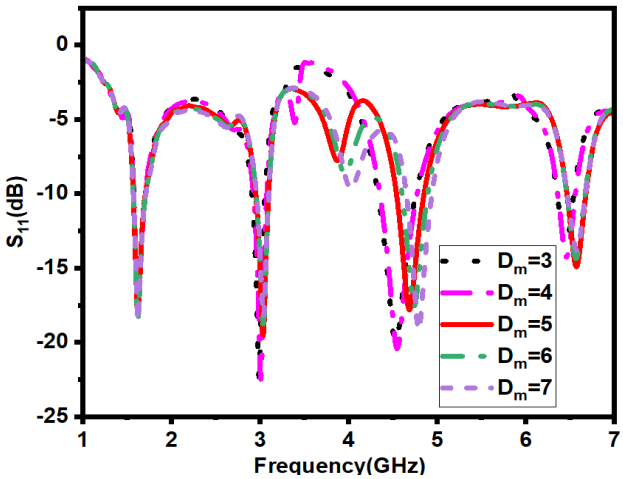

FIGURE 12. Impact of position of DRA over feedline "D_m" on reflection coefficient.

interference is employed. A Vector Network Analyzer (VNA) is used for the measurements and accurate characterization of the reflection coefficients, gain, and other significant characteristics. Fig. 13(a) depicts the fabricated prototype without DR, Fig. 13(b) shows the fabricated prototype with the DR while Fig. 13 (c) shows the fabricated prototype in the anechoic chamber setup for measuring the results.

B. SCATTERING PARAMETERS

Scattering parameters which include reflection coefficients of the proposed design are evaluated through simulation and measurement, as shown in Fig. 14. The simulated operating bands are 1.57—1.71 GHz, 2.95—3.1 GHz, 4.6—4.9 GHz and 6.46—6.6 GHz with 9.2%,5%,8.3%,5.6% fractional bandwidth respectively. Due to constructive interference within the measuring facility, the measured percentage bandwidth is slightly enhanced with 9.4%, 6%, 9% and 5.77 % respectively. Overall, there is a close agreement between the simulated and measured results, indicating the validity of the design. However, some minor discrepancies in impedance matching are observed. This can be attributed to fabrication inaccuracies and imperfections in the measuring environment. Despite these discrepancies, the general agreement between the simulated and measured reflection coefficients validates the design's performance.

C. SIMULATED AND MEASURED GAIN

The performance and effectiveness of an antenna capacity to radiate and transmit power are strongly influenced by its gain and efficiency characteristics. Fig. 15 shows the evaluation of the gain of the proposed design over different operating bands using simulation and measurement. The simulated gain of proposed design at 1.62 GHz, 3.03 GHz, 4.7 GHz and 6.5 GHz are 1.4 dBi, 1.8 dBi, 2.1dBi and 2dBi while measured value of gain are 1.5 dBi, 1.9 dBi, 2.3 dBi and 2.1 dBi, respectively.

MOST WIEDZY Downloaded from mostwiedzy.pl

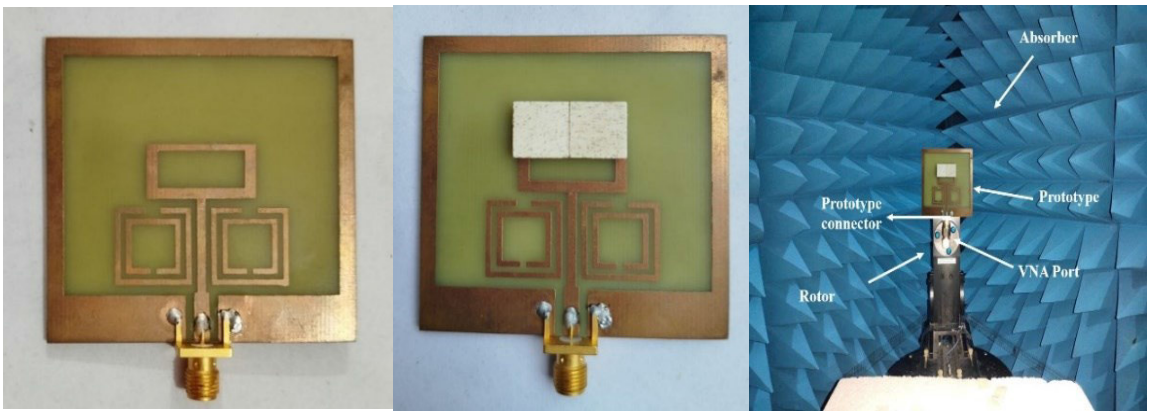

(a) (b) (c)

FIGURE 13. Fabricated design top view (a) without DRA (b) with DRA (c) fabricated design in anechoic chamber measurement facility.

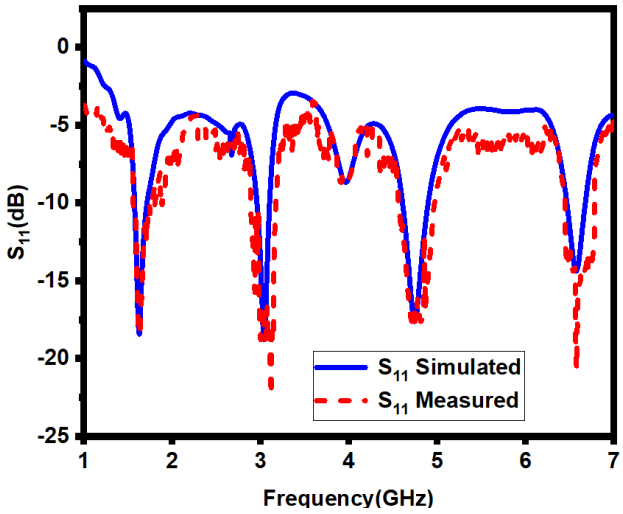

FIGURE 14. Simulated and Measured reflection coefficients of the proposed design.

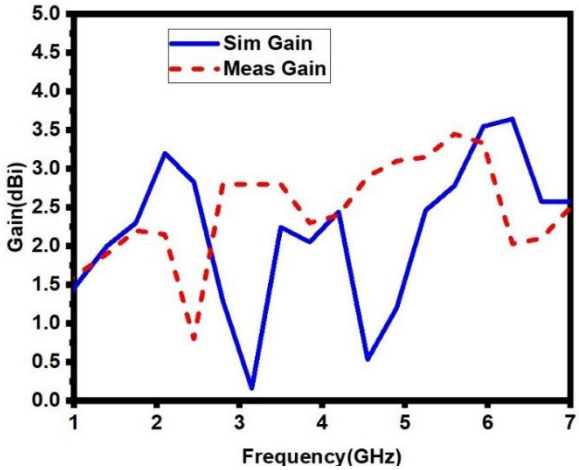

FIGURE 15. Simulated and measured gain of the proposed design over the operating bands.

Overall, the simulated gain values for the lower and higher operating bands closely agree with the measured results. Fabrication tolerances and measurement errors are just two reasons for this mismatch in the simulated and measured results. In addition, the high values of the measured gain may attribute to the constructive interference in the anechoic chamber. The broad consistency between the simulated and measured gains, despite this little variation, shows that the design is successful in providing the desired radiation properties. Table 2 summarizes the simulated and measured gain as well as percentage bandwidth at all operating frequencies.

D. CURRENT DISTRIBUTION

Overall design consists of two resonant structures (hybrid DR and SRRs). The surface current distribution helps which portion of SRR has active current distribution and what are the operating modes with in the DR at the specific resonance frequencies. Thus, it highly helps to control those resonance frequencies by varying the variables of the SRR and DR. The lower frequencies are due to the current distribution on the SRRs. It is important to note that based on DWM theory details, the higher frequency resonances are attributed to the multiple operating TE modes with in the DR [36]. Fig. 16 highlights the current distribution patterns at specific frequencies both on the SRRS and DR. At 1.62 GHz, as shown in Fig. 16(a), the current is uniformly distributed along the inner SSR, while it is concentrated on the lower parts of the outer SSR. At 3.03 GHz, as shown in Fig. 16(b), the current is focused on upper part of the inner and outer SSRs. This current distribution pattern indicates a balanced current flow within the design, contributing to the desired resonance at this frequency. Two resonance frequencies i-e 4.7 and 6.56 GHz are due to the two active operating modes with in the DR. At 4.7 GHz (Fig. 16(c)), the electric field distribution in XY and YZ surfaces of DRA confirms TE_{20} operating mode while at 6.56 GHz (Fig. 16(d)), XY and YZ surface of the DR electric field orientation confirms quasi $TE_{21\delta}$ operating mode.

MOST WIEDZY Downloaded from mostwiedzy.pl

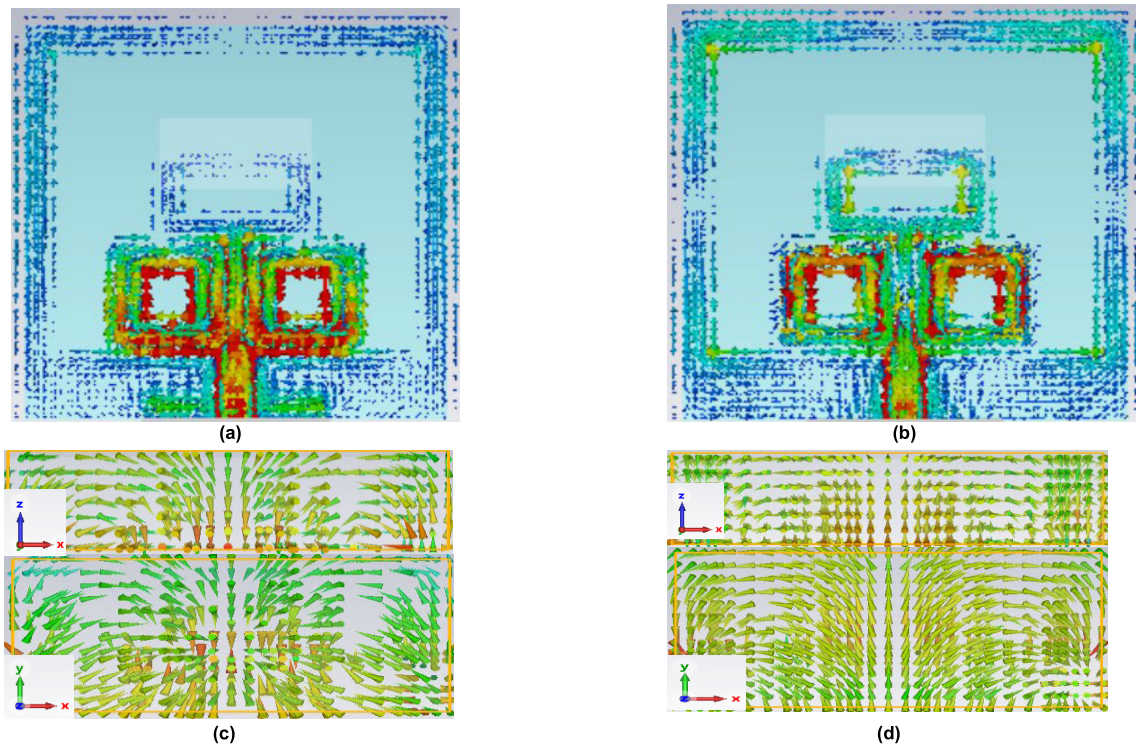

FIGURE 16. Surface current distribution at (a) 1.62GHz (b) 3.03GHz and electric field distribution on the DR at (c) 4.7 GHz, (d) 6.56GHz.

TABLE 2. Detail of simulated and measured gain.

Sr. no.	*Resonance Frequency (GHz)*	*Operating bandwidth (GHz)*	*Bandwidth (%)*	*Simulated Gain(dBi)*	*Measured Gain(dBi)*
1	1.62	1.57—1.71	9.2	1.4	1.5
2	3.03	2.95—3.1	5	1.8	1.9
3	4.7	4.6—4.9	8.3	2.1	2.3
4	6.56	6.46—6.6	5.3	2.0	2.1

E. FAR FIELD RADIATION PATTEREN

Fig. 17(a-d) details the far-field radiation patterns in terms of electric field (XY-plane) and magnetic field (YZ-plane) respectively. There is a strong correlation between the omnidirectional nature of the radiation patterns observed in simulations and measurements. It is important to note that imperfect production processes and unfavorable testing environments could cause minor variations at 3.03 GHz between simulated and measured radiation patterns. The antenna's performance at specific frequencies may vary slightly as a result of these considerations. The fabricated prototype is shown in Fig. 13(c), arranged inside the measuring device for measuring far-field radiation patterns, guaranteeing accurate evaluation of the radiation characteristics of the antenna.

Although majority of the simulated and measured results are in close agreement, however additional potential source of deviation between the simulated by measured results arise due to environmental factors and limitations in the experimental setup. These include reflection from surrounding objects, temperature and humidity variation, manufacturing variability. Moreover, instrumentation limitations, calibration issues, cable losses and connectors orientation are some additional reasons for this deviation. Controlling these factors may further enhance the correlation between the simulated and measured results.

F. SIMULATED TIME DOMAIN ANALYSIS

When designing and analyzing the proposed antenna system, group delay is crucial, particularly for applications that require high precision and minimal signal distortion. Group delay, which can have an impact on communication system performance, is the term used to describe the spatial delay that a signal experiences as it travels through the antenna. Group delay is defined as the derivative of the phase response of the system with respect to angular frequency [37]:

$$\tau_g(\omega) = -\frac{d\phi(\omega)}{d\omega} \tag{23}$$

where $\tau_g(\omega)$ is the group delay, $\phi(\omega)$ is the phase response and ω is the angular frequency. For DRA operating in the sub-6 GHz range, the group delay is typically in the order of nanoseconds (ns). Our analysis primarily focuses on orientations that are representative of typical deployment scenarios, providing a realistic perspective on the expected

MOST WIEDZY Downloaded from mostwiedzy.pl

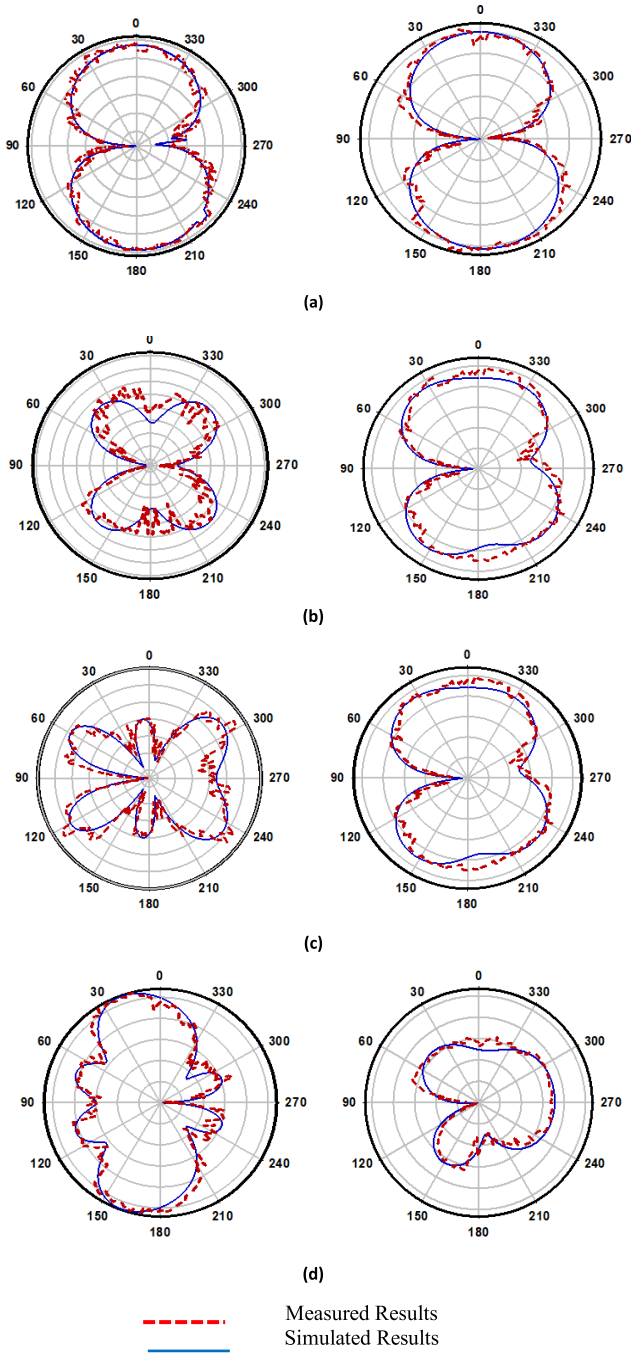

FIGURE 17. Radiation pattern E-Field(left) and H-Field(right) of the proposed design at (a) 1.62GHz, (b) 3.03GHz, (c) 4.7 GHz and (d) 6.56GHz respectively.

performance. For many applications, such as those in wireless communication and satellite links, the main beam direction is typically aligned with the primary signal path, making these orientations most relevant. As such, the provided data accurately reflects the antenna's practical performance under standard conditions.

Fig. 18 shows two orientations: face-to-face and side-by-side. For both the orientations, the designs were isolated at a distance of 382 mm (2 times λ_0 at 1.57 GHz) to create a far field atmosphere. As shown in the figure, ant-1 acts as a

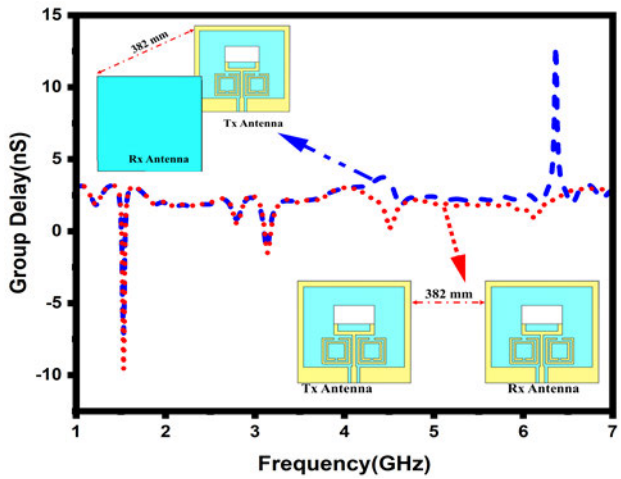

FIGURE 18. Shows the design orientations and simulated results of the calculated group delay.

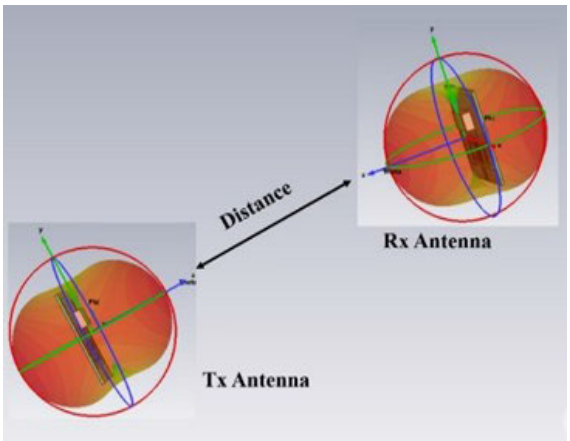

FIGURE 19. Virtual LOS environment demonstrating the path loss and link budget estimation for a communication system.

transmitter and ant-2 as a receiver. It is seen that at 1.62 GHz, 3.03 GHz, 4.7 GHz and 6.56 GHz resonance frequencies, the values of group delay are 3 ns, 2.1 ns, 2 ns and 2.7 ns respectively, which implies minimal distortion.

V. LINK BUDGET ANALYSIS

This section explains the link budget analysis at various data rates, demonstrating the designed antenna wireless communication capacity, at various resonance frequencies. Transmitting stored data, changing device settings, and getting real-time data for crucial monitoring are all possible with a strongly established communication link. For far-field communication, the link margin needs to be greater than 0 dB [38]. As a result, the effectiveness of the proposed antenna is assessed in a virtual line-of-sight (LOS) free-space environment, as shown in Fig. 19. A positive value for link margin is required; common values might be anything between 3 to 20 dB [38]. A suitable link margin gives the system some resilience against uncontrollable factors that can impair system performance and quality of service, such as weather-related signal fading, mobile user

MOST WIEDZY Downloaded from mostwiedzy.pl

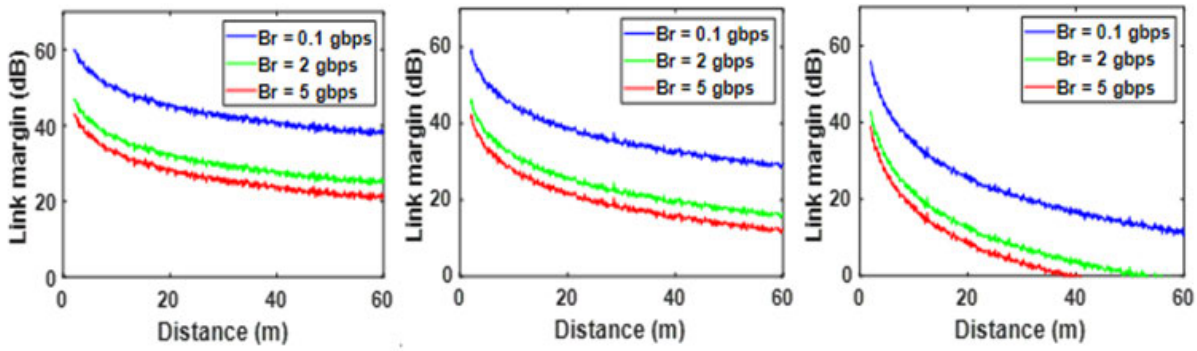

(a) n=1.5 (b) n=2 (c) n= 3

FIGURE 20. Calculated link margin for 1.62 GHz over varied bit rates.

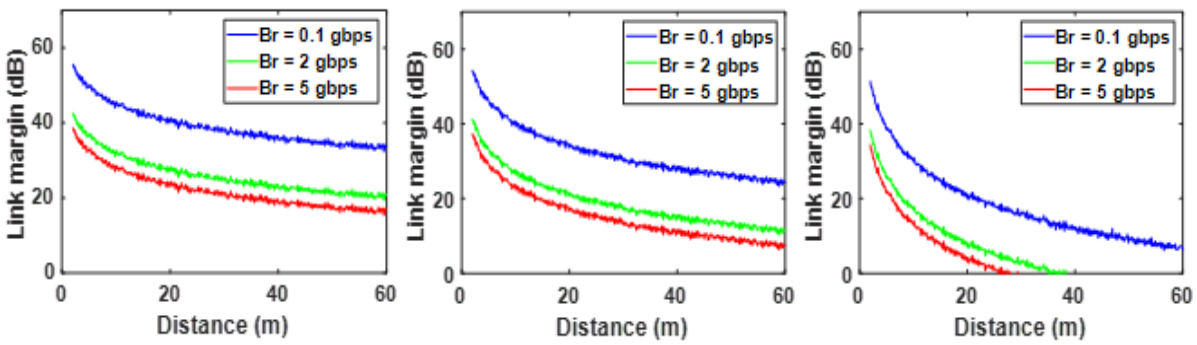

(a) n= 1.5 (b) n= 2 (c) n = 3

FIGURE 21. Calculated link margin for 3.03 GHz over varied bit rates.

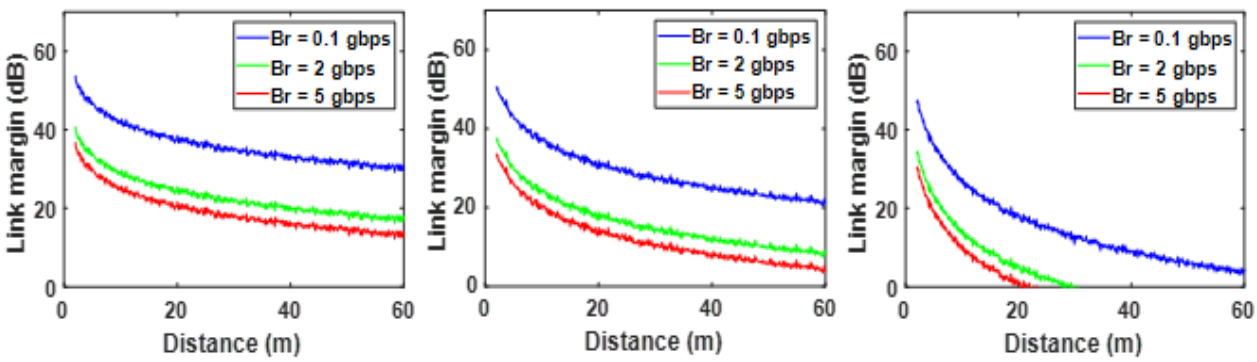

(a) n= 1.5 (b) n= 2 (c) n = 3

FIGURE 22. Calculated link margin for 4.7 GHz over varied bit rates.

mobility, multipath propagation issues, and other unforeseen events [39]. The RX antenna is continuously moved from 1 m to 80 m, whereas the TX antenna stays fixed in this test scenario. This displacement makes it possible to evaluate link budget requirements and research path loss [40], [41], [42].

$$Link\ Margin\ (dB) = Link\frac{C}{N_o} - Required\frac{C}{N_o} \tag{24}$$

$$LM\ (dB) = P_t + G_t - L_f + G_r - N_o - \frac{E_b}{N_O} - 10log_{10}B_r \tag{25}$$

Fig. 20 illustrates the link margin of the proposed antenna system. It is important to note that path loss exponent 'n' over varied bit rates is 1.5 for free space, 2 for line of sight communication and 3 for non-line of sight communication. The link margin is calculated for three bit rates, which are 0.1 Gbps, 2 Gbps, and 5 Gbps. The corresponding link margin verses distance plot is obtained for 1.62 GHz frequency as shown in Fig. 20. This figure shows that a 5 Gbps data rate can only be supported up to 60 m for free space communication with a link margin of 20 dB. At 2 Gbps, which is a lower data rate, the distance increases to over 60 m. Additionally, with a 0.1 Gbps lower data rate, communication is still feasible at a

MOST WIEDZY Downloaded from mostwiedzy.pl

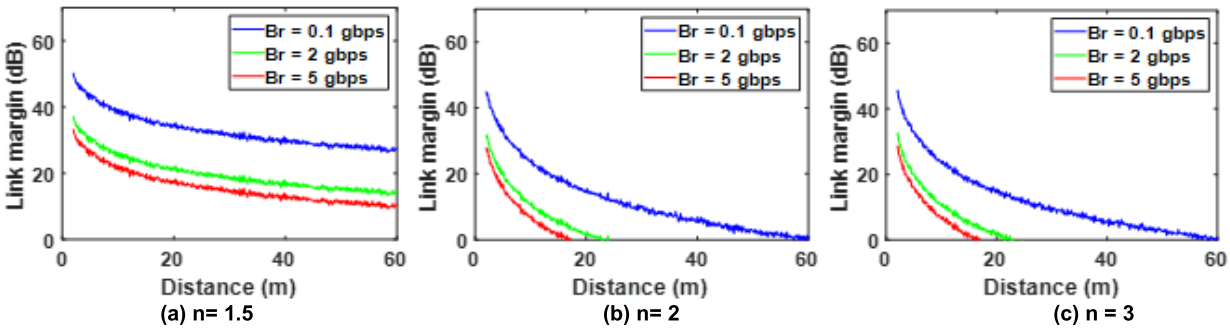

FIGURE 23. Calculated link margin for 6.56 GHz over varied bit rates.

TABLE 3. Comparison table of the proposed antenna with the related state of the art work.

Ref	Size(mm^3)	Size (λ^3)	Freq. Range (GHz)	No. of bands	BW (%)	Gain (dBi)	Link Budget Analysis	Time Domain Analysis
[5]	40×40×14.6	0.36×0.36×0.13	2.5-2.76,3.38-3.54, 4.9-5.3, 5.5-5.61, 5.78-5.98	5	9.9,4.6, 7.8, 2,3.4	1.2,3.1,2.4,3, 2.3	NA	No
[8]	36×37×1.6	0.4×0.45×0.01	3.45-3.55,5.97-6.1	2	2.8,2.84	3.83,0.57	NA	No
[9]	83*56*1.56	0.6×0.42×0.01	2.27-2.65,3.41-3.60,5.40-5.7	3	14,5,4	3.8,3.7,3.6	NA	No
[20]	47×50	0.61×0.65	3.95-4.24, 5.18-5.85,	2	7,12	2.3	NA	NA
[24]	70×51.6×1.8	0.8×0.6×0.02	3.5, 4.5, 5.8	3	3, 2.3, 4	1.1, 3.4, 5.1	NA	No
[25]	20×30×1.5	0.25×0.37×0.02	3.85, 4.71	2	2.5, 3	2.35, 2.69	NA	No
[27]	56×49×1.6	0.45×0.4×0.02	2.4, 3.4, 5.27	3	2.3, 4.6, 1.28	4.2, 4.6, 3.7	NA	No
[43]	32×32×14.8	0.3×0.3×0.12	2.25, 2.8, 4.5, 5.6-6.75	4	3.7,8.5,5.3,18		NA	No
[44]	14×30×8	0.23×0.5×0.13	3.24-4.34, 4.54-5.28, 5.64-6.00	3	29,15,6.2	1.3, 2, 1.6	NA	No
[45]	30 ×16.7	0.18×0.33	2.48-4.33	1	56	2.36	NA	No
[46]	23×10.8	0.27×0.13	3.3-3.6	1	23	2.26	NA	No
[47]	35×10	0.31×0.09	2.31–2.67, 4.90–5.56	2	14.46, 14.76	0.85, 1.67	NA	No
This work	**55×56×1.6**	**0.2×0.2×0.08**	**1.57-1.71,2.9-3.1, 4.6-4.89,6.46-6.67**	**4**	**9.2,5,8.3,5.6**	**1.5, 1.9, 2.3, 2.1**	**Yes**	**Yes**

distance of more than 60 m. Fig. 20(b) shows that a 5 Gbps data rate is only supported up to a distance of 20 m for LOS communication with a link margin of 20 dB. However, the distance increases to 40 m for a lower data rate of 2 Gbps. Furthermore, transmission is feasible across a distance of more than 60 m at a reduced data rate of 0.1 Gbps. Fig. 20(c) indicates that for NLOS communication for link margin of 20 dB, 5 Gbps data rate is supported only up to 8 m of distance. However, for a reduced data rate of 2 Gbps, the distance is increased to 15 m. Further, a reduced data rate of 0.1 Gbps, communication is possible to a distance of approximately 50 m.

Fig. 21 shows link budget analysis at 3.03GHz. Fig. 21(a) explains the free space communication for a link margin of 20 db. It is clear that 5 Gbps data rate is supported only up to distance of 30 m. However, for a reduced data rate of 2 Gbps, the distance is increased to 50 m. Further, a reduced data rate of 0.1 Gbps, communication is possible to a distance of more than 60 m. Fig. 21(b) shows that a 5 Gbps data rate is only supported up to a distance of 18 m for LOS communication with a link margin of 20 dB. However, the distance increases to 38 m for a lower data rate of 2 Gbps. Additionally, communication is feasible across a distance of more than 60 m at a 0.1 Gbps. Fig. 21(c) shows that a 5 Gbps data rate is only supported up to a distance of 5 m for NLOS communication with a link margin of 20 dB. However, the distance increases to 10 m for a lower data rate of 2 Gbps. Additionally, communication is feasible up to a distance of about 40 m at a 0.1 Gbps data rate.

Fig. 22 shows link budget analysis at 4.7 GHz. Fig. 22(a) indicates that for free space communication and for a link margin of 20 dB, 5 Gbps data rate is supported only up to 40 m of distance. However, for a reduced data rate of 2 Gbps, the distance is increased to 50 m. Further, a reduced data rate

MOST WIEDZY Downloaded from mostwiedzy.pl

of 0.1 Gbps, communication is possible to a distance of more than 60 m. Fig. 22(b) indicates that for LOS communication for link margin of 20 dB, 5 Gbps data rate is supported only up to 10 m of distance. However, for a reduced data rate of 2 Gbps, the distance is increased to 22 m. Further, a reduced data rate of 0.1 Gbps, communication is possible to a distance of approximal 60 m. Fig. 22(c) indicates that for NLOS communication for link margin of 20 dB, 5 Gbps data rate is supported only up to 5 m distance. However, for a reduced data rate of 2 Gbps, the distance is increased to 8 m. Further, a reduced data rate of 0.1 Gbps, communication is possible to a distance of approximately 20 m.

Fig. 23 shows link budget analysis for 6.56 GHz. Fig. 23(a) deals with free space communication, confirming that for a link margin of 20 dB, 5 Gbps data rate is supported only up to a distance of 10 m. However, for a reduced data rate of 2 Gbps, the distance is increased to 20 m. Further, a reduced data rate of 0.1 Gbps, communication is possible to a distance of more than 60 m. Fig. 23(b) shows that a 5 Gbps data rate is only supported up to a distance of 10 m for LOS communication with a link margin of 20 dB. With a 2 Gbps lower data rate, the distance is now 22 m. Additionally, communication is feasible up to a distance of 60 m at a 0.1 Gbps data rate. 5 Gbps data rate is only supported up to a distance of 3 m for NLOS communication with a link margin of 20 dB, as shown in Fig. 23(c). Nonetheless, the distance rises to 10 m with a 2 Gbps lower data rate. Additionally, at a 0.1 Gbps data rate, communication is feasible up to about 18 m. It can be concluded that with reduced data rates, the corresponding link margin can be increased and communication link can be established for longer distances.

The detailed link margin analysis shows that the designed antenna is highly suitable for wireless communication applications at various target operating frequencies.

Table 3 provides a thorough comparison of the aimed research with previously published studies. A number of important factors are compared, including electrical and physical dimensions, percentage fractional bandwidth, the number of working bands, efficiency and maximum gain. From the comparison, it is evident that the proposed work offers a compact size while delivering impressive performance characteristics. The antenna design achieves a smaller electrical and physical size while offering more operating bands as compared to the published studies, indicating its potential for space constrained applications.

VI. CONCLUSION

A compact rectangular SRR based RDRA along with a rectangular shaped feedline has been successfully designed, simulated, fabricated and tested. The proposed DRA demonstrates excellent performance characteristics and versatility for multiband wireless applications. Through the integration of SRRs, the DRA achieves resonance at four distinct frequency bands, i.e., 1.62 GHz, 3.03 GHz, 4.7 GHz and 6.56 GHz, with -10 dB impedance bandwidths of 9.2%, 5%, 8.3%, and 5.6%, respectively. The fabricated prototype aligns closely with the simulated results, confirming the suitability and reliability of the SRR-based DRA design. With its compact size, high performance, and the provision of four operating bands, the proposed design holds promise for various wireless applications. The proposed multiband SISO design can be extended to MIMO arrangement with circular polarization features by trying some additional structures and feeding mechanisms. The link budget analysis has confirmed the wireless communication reliability of the proposed design, thereby making it a potential candidate for future communications.

REFERENCES

[1] J. G. Andrews, S. Buzzi, W. Choi, S. V. Hanly, A. Lozano, A. C. K. Soong, and J. C. Zhang, "What will 5G be?" *IEEE J. Sel. Areas Commun.*, vol. 32, no. 6, pp. 1065–1082, Jun. 2014.

[2] G. Bakshi, A. Vaish, and R. S. Yaduvanshi, "Two-layer sapphire rectangular dielectric resonator antenna for rugged communications," *Prog. Electromagn. Res. Lett.*, vol. 85, pp. 73–80, 2019.

[3] U. Ullah, M. F. Ain, and Z. A. Ahmad, "A review of wideband circularly polarized dielectric resonator antennas," *China Commun.*, vol. 14, no. 6, pp. 65–79, 2017.

[4] H.-M. Chen, Y.-K. Wang, Y.-F. Lin, S.-C. Lin, and S.-C. Pan, "A compact dual-band dielectric resonator antenna using a parasitic slot," *IEEE Antennas Wireless Propag. Lett.*, vol. 8, pp. 173–176, 2009.

[5] A. Sharma, P. Ranjan, and R. K. Gangwar, "Multiband cylindrical dielectric resonator antenna for WLAN/WiMAX application," *Electron. Lett.*, vol. 53, no. 3, pp. 132–134, Feb. 2017.

[6] A. Gupta and R. K. Gangwar, "New excitation scheme to excite higher-order radiating modes in rectangular dielectric resonator antenna for microwave applications," *J. Microw. Power Electromagn. Energy*, vol. 52, no. 3, pp. 240–251, Jul. 2018.

[7] P. Kshirsagar, S. Gupta, and B. Mukherjee, "Novel design of conformalstrip excited asymmetrical rectangular dielectric resonator antenna for ultra-wide band application," *J. Microwave Power Electromagn. Energy*, vol. 52, no. 2, pp. 128–141, 2018.

[8] S. K. Noor, M. Jusoh, T. Sabapathy, A. H. Rambe, H. Vettikalladi, A. M. Albishi, and M. Himdi, "A patch antenna with enhanced gain and bandwidth for Sub-6 GHz and Sub-7 GHz 5G wireless applications," *Electronics*, vol. 12, no. 12, p. 2555, Jun. 2023.

[9] A. Pandya, T. K. Upadhyaya, and K. Pandya, "Tri-band defected ground plane based planar monopole antenna for Wi-Fi/WiMAX /WLAN applications," *Prog. Electromagn. Res. C*, vol. 108, pp. 127–136, 2021.

[10] S. Dhar, K. Patra, R. Ghatak, B. Gupta, and D. R. Poddar, "A dielectric resonator-loaded Minkowski fractal-shaped slot loop heptaband antenna," *IEEE Trans. Antennas Propag.*, vol. 63, no. 4, pp. 1521–1529, Apr. 2015.

[11] Z. Weng, X. Wang, Y. Jiao, and F. Zhang, "CPW-fed dielectric resonator antenna for ultra-wideband applications," *Microw. Opt. Technol. Lett.*, vol. 52, no. 12, pp. 2709–2712, Dec. 2010.

[12] K. S. Ryu and A. A. Kishk, "UWB dielectric resonator antenna having consistent omnidirectional pattern and low cross-polarization characteristics," *IEEE Trans. Antennas Propag.*, vol. 59, no. 4, pp. 1403–1408, Apr. 2011.

[13] H. Nawaz, S. Shahid, and G. G. Gentili, "Wideband dielectric resonator antenna using CPW fed segments," *Microw. Opt. Technol. Lett.*, vol. 58, no. 2, pp. 441–445, Feb. 2016.

[14] Y. Gao, Z. Feng, and L. Zhang, "Compact CPW-fed dielectric resonator antenna with dual polarization," *IEEE Antennas Wireless Propag. Lett.*, vol. 10, pp. 544–547, 2011.

[15] S. F. Roslan, M. R. Kamarudin, M. Khalily, and M. H. Jamaluddin, "An MIMO rectangular dielectric resonator antenna for 4G applications," *IEEE Antennas Wireless Propag. Lett.*, vol. 13, pp. 321–324, 2014.

[16] S. Bhattacharya and B. Gupta, "A novel multifrequency hybrid antenna," *Microw. Opt. Technol. Lett.*, vol. 55, no. 11, pp. 2712–2715, Nov. 2013.

[17] H. Nawaz and M. A. B. Abbasi, "Wide-band dielectric resonator antenna using K-shaped fractal," *Microw. Opt. Technol. Lett.*, vol. 58, no. 6, pp. 1504–1507, Jun. 2016.

[18] P. R. Girjashankar and T. K. Upadhyaya, "Surface mountable multiband dielectric resonator antenna for wireless communication systems," *Prog. Electromagn. Res. M*, vol. 103, pp. 173–183, 2021.

MOST WIEDZY Downloaded from mostwiedzy.pl

[19] A. Gupta and R. K. Gangwar, "Hybrid rectangular dielectric resonator antenna for multiband applications," *IETE Tech. Rev.*, vol. 37, no. 1, pp. 83–90, Jan. 2020.

[20] S. Khan, H. Ali, R. Khan, S. N. K. Marwat, H. Ramenah, and C. Tanougast, "Multi band frequency reconfigurable dielectric resonator antenna for multiple wireless application," in *Proc. 2nd Int. Conf. Commun., Comput. Digit. Syst. (C-CODE)*, Mar. 2019, pp. 73–76.

[21] S. Dhar, R. Ghatak, B. Gupta, and D. R. Poddar, "A wideband Minkowski fractal dielectric resonator antenna," *IEEE Trans. Antennas Propag.*, vol. 61, no. 6, pp. 2895–2903, Jun. 2013.

[22] M. Khalily, M. R. Kamarudin, M. Mokayef, S. Danesh, and S. E. Ghahferokhi, "A new wideband circularly polarized dielectric resonator antenna," *Radioengineering*, vol. 23, no. 1, pp. 175–180, Apr. 2014.

[23] R. Banuprakash, G. Amith, G. S. P. N. Amith, N. Gagana, A. G. Raviand, and C. Pavanashree, "Design of multiband antenna for WiMAX and WLAN applications using DGS," *Int. J. Eng. Technol.*, vol. 7, no. 3.12, p. 140, Jul. 2018.

[24] R. Azim, A. M. H. Meaze, A. Affandi, M. M. Alam, R. Aktar, M. S. Mia, T. Alam, M. Samsuzzaman, and M. T. Islam, "A multi-slotted antenna for LTE/5G Sub-6 GHz wireless communication applications," *Int. J. Microw. Wireless Technol.*, vol. 13, no. 5, pp. 486–496, Jun. 2021.

[25] B. Huang, M. Li, W. Lin, J. Zhang, G. Zhang, and F. Wu, "A compact slotted patch hybrid-mode antenna for sub-6 GHz communication," *Int. J. Antennas Propag.*, vol. 2020, no. 1, 2020, Art. no. 8262361.

[26] R. Manish, E. H. Reddy, B. Anusha, M. N. S. Prasad, P. Mishra, and Dr. K. D. Kulat, "Design of multi-band patch antenna for 5G, WiFi, Bluetooth, WiMax and WLAN applications," *Int. J. Eng. Res. Technol. (IJERT)*, vol. 11, no. 4, pp. 1–5, Apr. 2022.

[27] A. K. Panda, S. Sahu, and R. K. Mishra, "DRA gain enhancement using a planar metamaterial superstrate," *Int. J. RF Microwave Comput.-Aided Eng.*, vol. 28, no. 7, p. e21445, 2018.

[28] M. S. Khan, S. Khan, O. Khan, S. Aqeel, N. Gohar, and M. Dalarsson, "Mutual coupling reduction in MIMO DRA through metamaterials," *Sensors*, vol. 23, no. 18, p. 7720, Sep. 2023.

[29] N. F. Soliman, S. M. Abd-Alhalem, W. El-Shafai, S. Eldin S. E. Abdulrahman, N. Ismaiel, E.-S. M. El-Rabaie, A. D. Algarni, and F. E. Abd El-Samie, "Gain enhancement of dielectric resonator antenna using electromagnetic bandgap structure," *Comput., Mater. Continua*, vol. 71, no. 1, pp. 1613–1623, 2022.

[30] A. Sharma, G. Das, and R. K. Gangwar, "Design and analysis of tri-band dual-port dielectric resonator based hybrid antenna for WLAN/WiMAX applications," *IET Microw., Antennas Propag.*, vol. 12, no. 6, pp. 986–992, May 2018.

[31] H. Sarfraz, S. Khan, N. Khan, N. Gohar, S. A. A. Shah, J. Nasir, and M. Dalarsson, "Next-generation multiband wireless systems: A compact CSSR-based MIMO dielectric resonator antenna approach," *IEEE Access*, vol. 12, pp. 4910–4924, 2024.

[32] F. Bilotti, A. Toscano, and L. Vegni, "Design of spiral and multiple split-ring resonators for the realization of miniaturized metamaterial samples," *IEEE Trans. Antennas Propag.*, vol. 55, no. 8, pp. 2258–2267, Aug. 2007.

[33] S. Mehta and A. N. Abougreen, *Metamaterial Technology and Intelligent Metasurfaces for Wireless Communication Systems*. Hershey, PA, USA: IGI Global, 2023.

[34] J. D. Baena, J. Bonache, F. Martin, R. M. Sillero, F. Falcone, T. Lopetegi, M. A. G. Laso, J. Garcia-Garcia, I. Gil, M. F. Portillo, and M. Sorolla, "Equivalent-circuit models for split-ring resonators and complementary split-ring resonators coupled to planar transmission lines," *IEEE Trans. Microw. Theory Techn.*, vol. 53, no. 4, pp. 1451–1461, Apr. 2005, doi: 10.1109/TMTT.2005.845211.

[35] M. N. Hamza, M. T. Islam, and S. Koziel, "Advanced sensor for non-invasive breast cancer and brain cancer diagnosis using antenna array with metamaterial-based AMC," *Eng. Sci. Technol., Int. J.*, vol. 56, Aug. 2024, Art. no. 101779.

[36] R. Kumar, A. Chandra, N. Mishra, and R. K. Chaudhary, "A frequency tunable dielectric resonator antenna with reduction of cross polarisation for wi MAX and sub 6 GHz 5 G applications," *Defence Sci. J.*, vol. 73, no. 4, pp. 475–486, Jul. 2023.

[37] A. Sharma, A. Sarkar, A. Biswas, and M. J. Akhtar, "Dual-band multiple-input multiple-output antenna based on half split cylindrical dielectric resonator," *J. Electromagn. Waves Appl.*, vol. 32, no. 9, pp. 1152–1163, Jun. 2018.

[38] S. Keyrouz and C. Diego, "Dielectric resonator antennas: Basic concepts, design guidelines, and recent developments at millimeter-wave frequencies," *Int. J. Antennas Propag.*, vol. 1, 2016, Art. no. 6075680.

[39] S. A. A. Shah, Y.-H. Lim, and H. Yoo, "A novel development of endovascular aortic stent system featuring promising antenna characteristics," *IEEE Trans. Antennas Propag.*, vol. 70, no. 3, pp. 2214–2222, Mar. 2022, doi: 10.1109/TAP.2021.3111200.

[40] S. A. A. Shah, A. Basir, Y.-H. Lim, and H. Yoo, "A novel efficient wirelessly powered biotelemetric endovascular aortic stent antenna system," *IEEE Trans. Antennas Propag.*, vol. 71, no. 9, pp. 7132–7145, Sep. 2023, doi: 10.1109/TAP.2023.3291419.

[41] P. Shariff B. G., A. A. Naik, T. Ali, P. R. Mane, R. M. David, S. Pathan, and J. Anguera, "High-isolation wide-band four-element MIMO antenna covering ka-band for 5G wireless applications," *IEEE Access*, vol. 11, pp. 123030–123046, 2023, doi: 10.1109/ACCESS.2023.3328777.

[42] K. Pedram, M. Naderi, F. S. Jafari, and F. B. Zarrabi, "Compact quad-band second harmonic antenna based on metamaterial DRA load," *Microw. Opt. Technol. Lett.*, vol. 61, no. 8, pp. 1938–1944, Aug. 2019.

[43] Q. Guo, J. Zhang, J. Zhu, and D. Yan, "A compact multiband dielectric resonator antenna for wireless communications," *Microw. Opt. Technol. Lett.*, vol. 62, no. 9, pp. 2945–2952, Sep. 2020.

[44] H. K. Polat, M. D. Geyikoglu, and B. Cavusoglu, "Modeling and validation of a new reconfgurable patch antenna through equivalent lumped circuit-based design for minimum tuning effort," *Microw. Opt. Technol. Lett.*, vol. 62, no. 6, pp. 2335–2345, 2020.

[45] N. Mishra, A. Gupta, and R. K. Chaudhary, "A compact CPW-fed wideband metamaterial antenna using Ωshaped interdigital capacitor for mobile applications," *Microw. Opt. Technol. Lett.*, vol. 57, no. 11, pp. 2558–2562, Nov. 2015.

[46] N. Mishra and R. K. Chaudhary, "A miniaturized ZOR antenna with enhanced bandwidth for WiMAX applications," *Microw. Opt. Technol. Lett.*, vol. 58, no. 1, pp. 71–75, Jan. 2016.

[47] J. K. Rai, K. Anuragi, N. Mishra, R. Chowdhury, S. Kumar, and P. Ranjan, "Dual-band miniaturized composite right left handed transmission line ZOR antenna for microwave communication with machine learning approach," *AEU—Int. J. Electron. Commun.*, vol. 176, Mar. 2024, Art. no. 155120.

SHAHID KHAN received the B.S. degree in telecommunication engineering from the University of Engineering and Technology Peshawar, Pakistan, the M.S. degree in satellite navigation and related applications from the Politecnico de Torino, Italy, in 2011, and the Ph.D. degree from the University of Lorraine, France, in 2021. He was a Visiting Fellow with the 5G Innovation Center, University of Surrey. Currently, he is a Research Assistant Professor with the Department of Electronics, Telecommunication and Computer Science, Gdánsk University of Technology, Poland. He is also working on the development of frequency selective surface, metamaterials design, circularly polarized phased array DRAs for satellite applications, implantable antennas, and reconfigurable dielectric resonator antenna for different wireless applications. He has published more than 48 articles in peer-reviewed journals and conferences. He is a Reviewer of IEEE Antennas and Wireless Propagation Letters, *Radio Science*, *Engineering Science and Technology, an International Journal*, *Results in Engineering*, *Physica Scripta*, *Ain Shams Engineering Journal*, and *Alexandria Engineering Journal*.

OWAIS KHAN received the B.Sc. degree in electrical engineering from the University of Engineering and Technology Peshawar, in 2017, and the master's degree in electrical engineering from the CECOS University of Information Technology and Emerging Sciences, Peshawar. He did research on MIMO during the master's degree. He conducted his research on MIMO antenna design for 5G. His research interests include MIMO antenna designs, phased array antenna designs, circularly antenna design, dielectric resonator antenna designs, phased array, mm-waves, wearable antennas, and implantable antennas.

MOST WIEDZY Downloaded from mostwiedzy.pl

KIRAN RAHEEL received the bachelor's degree in electrical engineering from the NWFP University of Engineering and Technology, Peshawar, Pakistan, in 2008, the M.S. degree in communication engineering, in 2013, and the Ph.D. degree in electrical engineering from the Department of Electrical Engineering, CECOS University of IT and Emerging Science, Peshawar, Pakistan. She is currently an Assistant Professor with the Electrical Engineering Department, CECOS University of IT and Emerging Sciences. Her research interests include in the field of wearable antennas, mm-Wave, MIMO, and miniaturized printed antennas.

SYED AHSON ALI SHAH (Member, IEEE) received the B.Sc. degree in telecommunication engineering from the University of Engineering and Technology, Pakistan, in 2015, and the Ph.D. degree in electronic engineering from Hanyang University, South Korea, in 2022. He was a Postdoctoral Researcher with Hanyang University, in 2022 and 2023, and currently with GIST. To date, he has published several journals and conference papers. His research interests include wireless communications, wireless power transfer, and synthesized magnetic field focusing. He has received IETE MN SAHA Memorial Award and Gold Medal for Best Application-Oriented Paper, in 2018. He has also received Bronze Paper Award at IEEE Student Paper Contest, Seoul, in 2019, 2021, and 2022. He has also won Third Best Student Paper Award, in 2021, Competition arranged by Korean Institute of Electromagnetic Engineering and Science (KIEES). His Ph.D. thesis has been recognized as one of the excellent dissertations and received the Best Ph.D. Thesis Award in overall university and the only in Electronic Engineering Department.

BILAL TARIQ MALIK received the B.Sc. and M.Sc. degrees in electrical engineering from the Department of Electrical and Computer Engineering, COMSATS University Islamabad, Pakistan, in 2011 and 2014, respectively, and the Ph.D. degree in electronics and electrical engineering from the University of Leeds, U.K., in 2019. Since 2023, he has been associated with COMSATS University Islamabad as an Assistant Professor. Currently, he is a Postdoctoral Researcher with Gdánsk University of Technology, Poland. His research interests include millimeter-wave antenna arrays, flexible printed circuits, intelligent reflective surfaces, and 5G + communications. He was awarded the Institute Silver Medal and the Campus Bronze Medal for the B.Sc. degree from COMSATS University Islamabad.

SALAHUDDIN KHAN is currently an Associate Professor with King Saud University. He is specialized in design, modeling, and simulation which can be extended to various fields of electronics, electromagnetic, and power systems, such as development of algorithms, realization of antenna devices, and power plant secondary systems. The above research lines have produced many research projects and publications. He has also contributed an U.S. patent.

NEELAM GOHAR received the Ph.D. degree from the University of Liverpool, U.K., in 2012. She had been the Head of the Department of Computer Science, Shaheed Benazir Bhutto Women University, Peshawar, for over eight years. She is currently an Assistant Professor. She is a reviewer of different journal and international conferences, organized national and international conferences, academic events, and resource person for different trainings; a member of different committees like establishment of Smart Classroom and Community College; a Technical Member of Online Readiness Committee and Post-Graduate Review Committee, focal person of different projects of HEC; a member of national curriculum revision committee in the field of IT, software engineering and computer science, recognized as an IT Professional by the Information and Communication Technology Council (ICTC) Canada; and participated in national and international training programs. She has published over more than 15 articles in international impact factor peer-reviewed journals. Her research interests include artificial intelligence, multi-agent systems, computational social choice theory, algorithmic game theory, data analytics, and data science.

SLAWOMIR KOZIEL (Fellow, IEEE) received the M.Sc. and Ph.D. degrees in electronic engineering from Gdańsk University of Technology, Poland, in 1995 and 2000, respectively, and the M.Sc. degree in theoretical physics and the M.Sc. and Ph.D. degrees in mathematics from the University of Gdańsk, Poland, in 2000, 2002, and 2003, respectively. He is currently a Professor with the Department of Technology, Reykjavik University, Iceland. His current research interests include the CAD and modeling of microwave and antenna structures, simulation-driven design, surrogate-based optimization, space mapping, circuit theory, analog signal processing, evolutionary computation, and numerical analysis.

MOST WIEDZY Downloaded from mostwiedzy.pl